Robust extraction of the proton charge radius from electron-proton scattering data

Xuefei Yan, Douglas W. Higinbotham, Dipangkar Dutta, Haiyan Gao, Ashot Gasparian, Mahbub A. Khandaker, Nilanga Liyanage, Eugene Pasyuk, Chao Peng, and Weizhi Xiong

Phys. Rev. C **98**, 025204 — Published 21 August 2018

DOI: 10.1103/PhysRevC.98.025204

Robust extraction of the proton charge radius from electron-proton scattering data

Xuefei Yan,[1,2,*] Douglas W. Higinbotham,[3] Dipangkar Dutta,[4] Haiyan Gao,[1,2,5] Ashot Gasparian,[6] Mahbub A. Khandaker,[7] Nilanga Liyanage,[8] Eugene Pasyuk,[3] Chao Peng,[1,2] and Weizhi Xiong[1,2]

[1] *Duke University, Durham, North Carolina 27708, USA*
[2] *Triangle Universities Nuclear Laboratory, Durham, North Carolina 27708, USA*
[3] *Thomas Jefferson National Accelerator Facility, 12000 Jefferson Avenue, Newport News, Virginia 23606, USA*
[4] *Mississippi State University, Mississippi State 39762, USA*
[5] *Duke Kunshan University, Jiangsu 215316, China*
[6] *North Carolina A&T State University, Greensboro, North Carolina 27411, USA*
[7] *Idaho State University, Idaho 83209, USA*
[8] *University of Virginia, Charlottesville, VA 22904, USA*

(Dated: July 22, 2018)

Background: To extract the proton charge radius from electron scattering data, requires determining the slope of the charge form factor at Q^2 of zero. As experimental data cannot reach that limit, numerous methods for making the extraction have been proposed.

Purpose: In this study, we seek to find functional forms that will allow for a robust extraction of the proton radius from a wide variety of functional forms. The primary motivation of this study is to have confidence in the extraction of upcoming low Q^2 experimental data.

Method: We create a general framework for studying various form-factor functions along with various fitting functions. The input form factors are used to generate pseudo-data with fluctuations mimicking the binning and random uncertainty of a set of real data. All combinations of input functions and fit functions can then be tested repeatedly against regenerated pseudo-data. Since the input radius is known, this allows us to find fitting functions that are robust for proton radius extractions in an objective fashion.

Results: For the range and uncertainty of the PRad data, we find that a two-parameter rational function, a two-parameter continued fraction and the second order polynomial expansion of z can extract the input radius regardless of the input charge form factor function that is used.

Conclusions: We have created a framework to determine which functional forms allow for a robust extraction of the radius from pseudo-data generated from a wide variety of trial functions. By taking into account both bias and variance, the optimal functions for extracting the proton radius can be determined.

I. INTRODUCTION

Much effort has been devoted to the determination of the charge radius of the proton (R), but results from different experiments and/or analyses exhibit sizable discrepancies. For example, in high-precision muonic hydrogen Lamb shift experiments, R was measured to be 0.8409 ± 0.0004 fm [1, 2], while the current value from CODATA, determined from atomic Lamb shift and electron-proton (ep) scattering experiments, is $R = 0.8751 \pm 0.0061$ fm [3]. This difference is known as the proton radius puzzle [4–6]. The newer atomic Lamb shift and electron scattering results that have become available [7–9] thus far are contradictory and the proton radius puzzle remains.

To extract the proton radius from ep-scattering data the electric form factor, G_E, is first plotted as a function of the four-momentum transferred squared, Q^2. This data must then be fit to find the slope at $Q^2 = 0$. The radius depends on the slope according to Eq. 1. Since experimental electron scattering cannot reach the $Q^2 = 0$ limit, many different methods have been proposed to extract the radius from the data.

$$R \equiv \left(-6 \left. \frac{\mathrm{d}G_E(Q^2)}{\mathrm{d}Q^2} \right|_{Q^2=0} \right)^{1/2} \tag{1}$$

Recent global analyses of ep-scattering data found $R \approx 0.84$ fm, in agreement with the muonic Lamb shift results [10–17]. Though these analyses used existing experimental data, they systematically extract smaller radii than the results of other groups [18–23]. It has been pointed out that the difference between the results is mainly due to differences in how the high-order moments $\langle r^{2n} \rangle$ ($n > 1$) are handled [24, 25]. A summary table of the higher order moments from a number of these fits can be found in the recent work of Alarcón and Weiss [26].

The form-factor G_E is often fit with a multi-parameter polynomial expansion of Q^2 up to an order Q^{2N}, since each moment $\langle r^{2n} \rangle$ ($1 \leq n \leq N$) corresponds to an independent parameter. Though this description seems to be model independent, as Kraus *et al.* have shown, it does not ensure a correct R extraction when it is used for extrapolating beyond the data to $Q^2 = 0$ [27].

In addition to multi-parameter polynomials, functional forms of G_E based on models of the proton charge distri-

* xy33@phy.duke.edu

bution are also used to determine R. The problem with this approach is that it can be difficult to quantify how much the extraction of R is affected by the assumptions in the model. In addition, constructing a model description of the full charge distribution of the proton is a far more complex problem than simply trying to mathematically extract R value from experimental data.

Herein we present a systematic method to find mathematical function(s) that can robustly extract R over a broad set of G_E input functions. In this study, we use the expected binning and uncertainty of the PRad experiment [28, 29] as an example, but the method can be applied to any expected binning and uncertainty.

II. METHOD

If the exact functional form of the proton's charge form factor, G_E, were available, one could fit experimental data to this same functional form and extract the charge radius. This ideal case is easily simulated by creating randomized pseudo-data and examining the fitting results R(fit) using the same functional form as was used to generate the pseudo-data. This process can be repeated multiple times in order to obtain a distribution of R(fit).

However, as the true functional form is unknown, one has to search for functional forms that can extract R by extrapolating to $Q^2 = 0$ from experimental data. For simplicity, we call this feature robustness. In fact, due to the variability of experimental data, the best fitting function may not even be the true functional form [30].

To find appropriate functions for a given binning and uncertainty, we generate pseudo-data using a wide variety of functional forms. Next, we systematically fit each set of pseudo-data with various functional forms. By studying the distributions of the results, we find functional forms that robustly extract the input radius. To be considered robust, the set of extracted R values must be, within errors, the same as the R value used to generate the pseudo-data regardless of which G_E parameterization was used in the generating function.

A program library has been built with three parts to generate pseudo data, add fluctuations, and fit the pseudo data [31]. This program library is coded in C++ using the Minuit and CERN ROOT package [32, 33]. The three components of this library are described in detail in the following subsections.

A. Generator

The generator library has been built to generate G_E values at given Q^2 using either simple standard functions, parameterizations of experimental data or full theoretical calculations. Other functions could easily be added to this library. The currently installed functions include:

a. Dipole The dipole functional form of G_E [34] is expressed as

$$G_E(Q^2) = \left(1 + \frac{Q^2}{p_1}\right)^{-2}, \tag{2}$$

where $p_1 = 12/R^2$. This functional form corresponds to an exponential charge distribution of the proton, and the relation between moments is

$$\langle r^{2n}\rangle = \frac{(n+1)(2n+1)}{6}\langle r^2\rangle\langle r^{2n-2}\rangle, \tag{3}$$

where $n > 1$.

b. Monopole The monopole functional form of G_E [34] is expressed as

$$G_E(Q^2) = \left(1 + \frac{Q^2}{p_1}\right)^{-1}, \tag{4}$$

where $p_1 = 6/R^2$. This functional form corresponds to a Yukawa charge distribution of the proton, and the relation between moments is

$$\langle r^{2n}\rangle = \frac{n(2n+1)}{3}\langle r^2\rangle\langle r^{2n-2}\rangle, \tag{5}$$

where $n > 1$.

c. Gaussian The Gaussian functional form of G_E [34] is expressed as

$$G_E(Q^2) = \exp(-Q^2/p_1), \tag{6}$$

where $p_1 = 6/R^2$. This functional form corresponds to a Gaussian charge distribution of the proton, and the relation between moments is

$$\langle r^{2n}\rangle = \frac{2n+1}{3}\langle r^2\rangle\langle r^{2n-2}\rangle, \tag{7}$$

where $n > 1$.

d. Kelly-2004 The parameterization from Ref. [35] is expressed as

$$G_E(Q^2) = \frac{1 + a_1\tau}{1 + b_1\tau + b_2\tau^2 + b_3\tau^3}, \tag{8}$$

where $\tau = Q^2/4m_p^2$, and m_p is the proton mass. The parameters a_1, b_1, b_2 and b_3 can be found in Table I of Ref. [35]. The radius in this parameterization is $R =$ 0.8630 fm.

e. Arrington-2004 The parameterization from Ref. [36] is expressed as

$$G_E(Q^2) = \left(1 + \sum_{i=1}^{N} p_{2i}Q^{2i}\right)^{-1}, \tag{9}$$

where parameters p_{2i} up to $i = 6$ can be found in Table I of Ref. [36]. The radius in this parameterization is $R = 0.8682$ fm.

f. Arrington-2007 The parameterization from Ref. [37] is a fifth-order continued-fraction (CF) expansion expressed as:

$$G_E(Q^2) = \frac{1}{1+\frac{p_1 Q^2}{1+\frac{p_2 Q^2}{1+\cdots}}}, \quad (10)$$

where the parameters p_i (index i from 1 to 5) can be found in Table I in Ref. [37]. The radius in this parameterization is $R = 0.8965$ fm.

g. Venkat-2011 The parameterization from Ref. [38] is expressed as

$$G_E(Q^2) = \frac{1 + a_1\tau + a_2\tau^2 + a_3\tau^3}{1 + b_1\tau + b_2\tau^2 + b_3\tau^3 + b_4\tau^4 + b_5\tau^5}, \quad (11)$$

where parameters a_i and b_i can be found in Table II of Ref. [38]. The radius in this parameterization is $R = 0.8779$ fm.

h. Bernauer-2014 This parameterization is a refit of the full set of 1422 data points from Ref. [23] and is expressed as a 10th-order polynomial expansion of Q^2:

$$G_E(Q^2) = 1 + \sum_{i=1}^{10} p_i Q^{2i}, \quad (12)$$

where the refitted parameters p_i are close to those found in appendix J.1 of Ref. [39]. The radius in this parameterization is $R = 0.8868$ fm.

i. Alarcón-2017 As a fully realistic charge form factor, we used the model of Alarcón and Weiss [26, 40, 41] referred to herein as Alarcón-2017. This model uses the recently developed method combining chiral effective field theory and dispersion analysis. Solely for the purpose of testing extraction techniques, the radius in the model was fixed to a series of values: 0.84 fm from muonic hydrogen, 0.875 fm from CODATA, and 0.85 fm as the central value from the range of radii allowed by the model. Unlike the other models where a simple function could be programmed, here we have used a finely spaced table of charge values and then fit it with a cubic spline. The spline function can then be called in a similar manner to the other functions.

j. Ye-2018 The parameterization of Ye *et al.* [42] is a fit to world data with the radius fixed to $R = 0.879$ fm. The parameterization and the values of the parameters can be found in the supplemental materials of Ref. [42]. The author Z. Ye also provided a separate parameterization with a different fixed radius, $R = 0.85$ fm. This second parameterization will be referred to as Ye-2018 (refix) in this study.

B. Fluctuation-adder

In order to mimic the variability of real data, library allows adding bin-by-bin and/or overall fluctuations to the G_E vs. Q^2 tables. It includes fluctuations according to a user-defined random Gaussian distribution, $\mathcal{N}(\mu, \sigma_g^2)$. In the bin-by-bin case, the uncertainty δG_E of each bin is defined by the user. The library sets $\mu = 0$ and $\sigma_g = \delta G_E$, and generates fluctuations according to $\mathcal{N}(\mu, \sigma_g^2)$ in each bin. In the overall case, the user can manually set the values of μ and σ_g, and the library generates an overall scaling factor according to $\mathcal{N}(\mu, \sigma_g^2)$ for all the bins in a table. Other types of fluctuations, such as uniform and Breit-Wigner, are also included in the library for test purposes.

C. Fitter

To study which function robustly extract R from the generated pseudo-data, a fitting routine has been developed. This library uses the Minuit package of CERN ROOT to fit the G_E vs. Q^2 tables with the functional forms listed below:

a. Dipole The dipole fitter is expressed as

$$f_{\text{dipole}}(Q^2) = p_0 G_E(Q^2) = p_0 \left(1 + \frac{Q^2}{p_1}\right)^{-2}, \quad (13)$$

where p_0 is a floating normalization parameter, and p_1 is a fitting parameter related to the radius $R = \sqrt{12/p_1}$.

b. Monopole The monopole fitter is given by

$$f_{\text{monopole}}(Q^2) = p_0 G_E(Q^2) = p_0 \left(1 + \frac{Q^2}{p_1}\right)^{-1}, \quad (14)$$

and $R = \sqrt{6/p_1}$.

c. Gaussian The Gaussian fitter has the form

$$f_{\text{Gaussian}}(Q^2) = p_0 G_E(Q^2) = p_0 \exp(-Q^2/p_1), \quad (15)$$

and $R = \sqrt{6/p_1}$.

d. Multi-parameter polynomial-expansion of Q^2 The fitter of the multi-parameter polynomial-expansion of Q^2 is written as

$$f_{\text{polyQ}}(Q^2) = p_0 G_E(Q^2) = p_0 \left(1 + \sum_{i=1}^{N} p_i Q^{2i}\right), \quad (16)$$

where p_0 is a floating normalization parameter, p_1 is a fitting parameter related to the radius by $R = \sqrt{-6p_1}$, parameters for higher order terms (p_i with $i > 1$) are free fitting parameters, and N is defined by the user.

e. Multi-parameter rational-function of Q^2 The fitter of the multi-parameter rational-function of Q^2 is expressed as

$$f_{\text{rational}}(Q^2) = p_0 G_E(Q^2) = p_0 \frac{1 + \sum_{i=1}^{N} p_i^{(a)} Q^{2i}}{1 + \sum_{j=1}^{M} p_j^{(b)} Q^{2j}}, \quad (17)$$

where p_0 is a floating normalization parameter, $p_i^{(a)}$ and $p_j^{(b)}$ are free fitting parameters, and radius can be found as $R = \sqrt{6(p_1^{(b)} - p_1^{(a)})}$. The orders N and M are defined by the user.

f. CF expansion The CF expansion fitter is expressed as [43]

$$f_{\rm CF}(Q^2) = p_0 G_E(Q^2) = p_0 \frac{1}{1+\frac{p_1 Q^2}{1+\frac{p_2 Q^2}{1+\cdots}}}, \quad (18)$$

where p_0 is a floating normalization parameter, p_i ($i > 0$) are free fitting parameters, and $R = \sqrt{6p_1}$. The user can define the maximum i of the expansion.

g. Multi-parameter polynomial-expansion of z The z-transformation is expressed as [19]

$$z = \frac{\sqrt{T_c + Q^2} - \sqrt{T_c - T_0}}{\sqrt{T_c + Q^2} + \sqrt{T_c - T_0}}, \quad (19)$$

where $T_c = 4m_\pi^2$, m_π is set to be 140 MeV (close to the π^0 mass as in Ref. [19]), and T_0 is a free parameter representing the point mapping onto $z = 0$ (T_0 is set to 0 in this study). With the new variable z, G_E can be parameterized as

$$f_{\rm polyz}(Q^2) = p_0 G_E(Q^2) = p_0 \left(1 + \sum_{i=1}^{N} p_i z^i\right), \quad (20)$$

where p_0 is a floating normalization parameter, p_1 is a fitting parameter related to the radius by $R = \sqrt{-3p_1/2T_c}$, p_i are free fitting parameters, and N is defined by the user.

III. TESTS OVER FULL RANGE OF THE PRAD KINEMATICS

We tested functions over the expected Q^2 range for the PRad experiment of $3 \times 10^{-4} < Q^2 < 0.072$ GeV^2, using bin-by-bin random uncertainties from 0.02% to 1.1%. The exact values used can be found online and are denoted as bin set one [44]. As an example, Fig. 1 shows pseudo-data generated with the dipole generator [R(input) = 0.85 fm] in the PRad binning fit using the dipole fitter. In the first panel, no fluctuation is added to the central values of G_E while the other panels show two of the many possible outcomes of adding random fluctuations to the pseudo-data. the same input parameters. As one might expect, when there is no fluctuation, the fit curve goes through all the pseudo-data points perfectly and the input R value is obtained. However, when there are fluctuations, the results of the fit can differ from the input.

In order to determine the distribution of possible outcomes, one needs to generate many sets of pseudo-data and perform fits for each set. This is done using the following procedure:

a. Generation First, one G_E model is used to generate pseudo-data (using the generator), at the bin centers of Q^2 that the user inputs into the program.

b. Fluctuation-adding Next, bin-by-bin and overall fluctuations are added to the G_E vs. Q^2 tables in a random manner (using the fluctuation-adder), to mimic the real data. The bin-by-bin uncertainties are taken from the bin-set file, and an overall scaling uncertainty of 5% (far larger than expected in the PRad result) is added in the tests to show that this method works even if there is such a big scaling uncertainty.

c. Fitting Finally, the G_E vs. Q^2 tables are fit with a number of functional forms (using the fitting library) to extract R from the pseudo-data with fluctuations.

The steps of generation, fluctuation-adding and fitting are repeated 150,000 times for each combination of generator and fit function. The 150,000 fitting results of R(fit) for each combination comprise a distribution with a central value R(mean) and a root-mean-square (RMS) width. As the fitting uncertainty of R, determined by Minuit (for each of the 150,000 fits) is very close to the RMS width of the R(fit) distribution, we will use the RMS values to represent the one-σ fitting-uncertainty.

A. Fits with simple-function models

Fig. 2 shows the R(fit) distributions of the dipole, monopole and Gaussian fits when the dipole generator is used [R(input) = 0.85 fm]. It is observed that when the dipole fitter is used, R(mean) $\approx R$(input), but when the monopole or Gaussian fitter is used, R(mean) significantly deviates from R(input).

Fig. 3 summarizes the fitting results using the dipole, monopole and Gaussian fitter, respectively, when nine generators covering nine of the G_E models describe in section II A. It is clear that the simplest functional forms are not able to provide a robust extraction of R over the full kinematic range of PRad bins, since for various input G_E models, the fitting uncertainty (σ) is smaller than the size of the bias [$\delta R = R$(mean) $- R$(input)]. We note that in this type of statistical analysis, bias is simply the mean offset from the input value and is not meant as a pejorative term. In fact, it is the trade-off between bias and variance that is at the heart of machine learning algorithms [45].

B. Fits with polynomial expansions of Q^2

Polynomial expansions have been widely used to fit G_E vs. Q^2 data, though concerns have been raised about extrapolating with polynomial functions [14–16, 24, 27]. Fig. 4 summarizes the fitting results using the polynomial-expansion fitter with $N = 1$, 2, 3 and 4, using again the nine generators covering various types of G_E models.

For the full range of the PRad data, the first-order polynomial fitter is clearly not robust as $|\delta R| > \sigma$ for all the input G_E models. The second-order polynomial is marginally robust, since $|\delta R| \approx \sigma$ is found for models

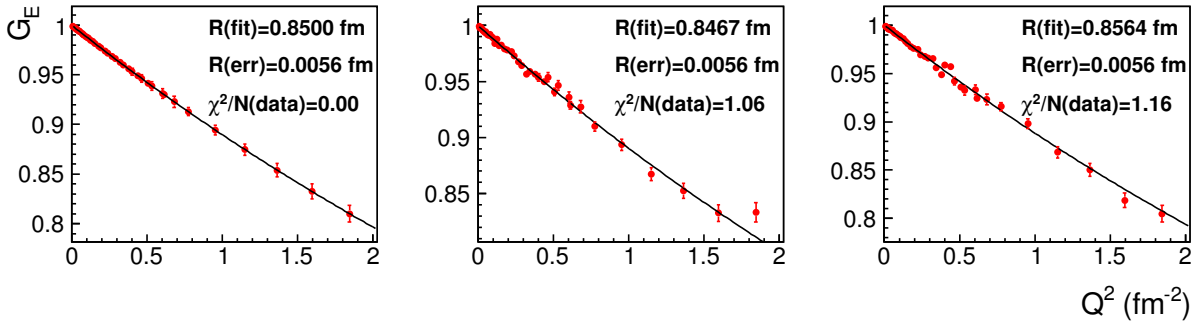

FIG. 1. (color online). Left panel shows pseudo-data generated with dipole functional form without fluctuations and the middle and right panel shows results with fluctuations [R(input) = 0.85 fm]. The fitting result [R(fit)], fitting uncertainty [R(err)] and χ^2 per data point [χ^2/N(data)] are presented in each panel.

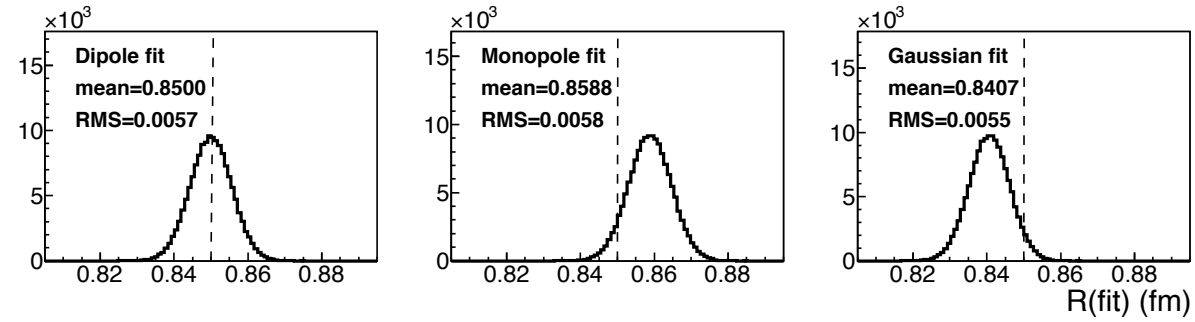

FIG. 2. Dipole, monopole and Gaussian fits of pseudo-data tables generated with the dipole functional form and added fluctuations. The dashed line indicates the value of the input radius of 0.85 fm.

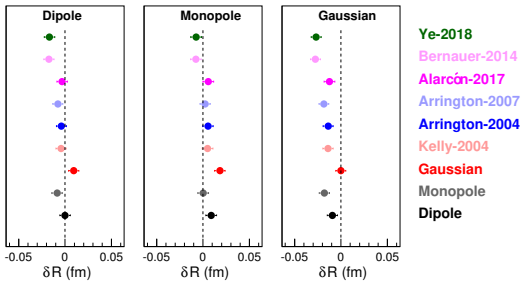

FIG. 3. (color online). Dipole, monopole and Gaussian fits of pseudo-data tables generated with nine models.

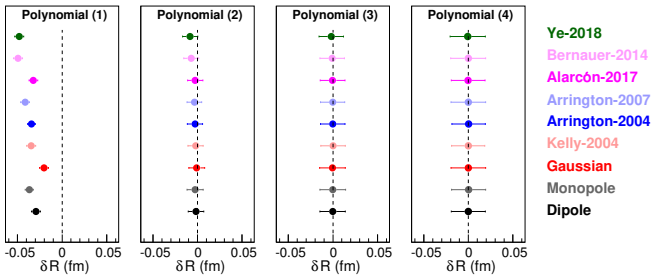

FIG. 4. (color online). Polynomial-expansion fits of pseudo-data tables generated with nine models.

Bernauer-2014 and Ye-2018, while $|\delta R| < \sigma$ is found for the others. The third and fourth order polynomial fits seem to be robust with $|\delta R| < \sigma$ for all the input G_E models, but with a significantly larger σ.

We observe that when the order of expansion is too low ($N = 1$), R(mean) is systematically and significantly smaller than R(input) for all the generators used in the tests. The polynomial (1) fit shows high bias and a low variance. When higher orders are included (N = 2, 3 and 4), R(mean) gets closer to R(input), regardless of the type of generator. At the same time, as the number of parameters increases the fitting uncertainties increases, showing low bias with high variance. The optimal choice of N depends on the Q^2 range, the distance between bin centers and the uncertainty level in the data table. This clearly illustrates the trade-off between bias and variance and the need to balanced them when fitting. Some efforts have been taken to build algorithms that automatically and systematically determine the proper order N when fitting certain data [15, 46].

C. Fits with rational functions of Q^2

Rational functions are also widely used to fit G_E vs. Q^2 data, such as in Refs. [35, 36, 38, 47]. Fig. 5 sum-

marizes the fitting results using the rational-function fitter with $(N, M) = (1, 1), (1, 2), (2, 1)$ and $(2, 2)$, using the same nine generators. In these tests, the rational-function fitter $(N, M)=(1, 1)$ extracts R robustly ($\delta R < 0.42\sigma$) regardless of the model parameterization in the generator. It also has the lowest fitting uncertainty among these four rational-function parameterizations. The higher order rational-function fitters, are also robust ($|\delta R| < \sigma$ for all input G_E models) but a have significantly larger fitting uncertainties.

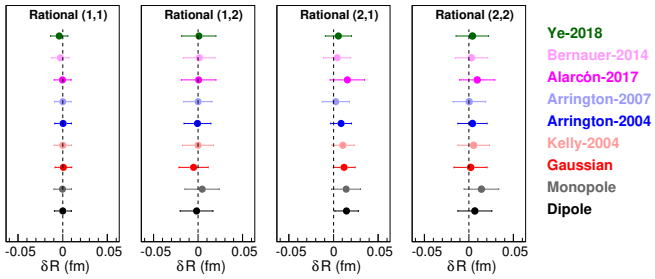

FIG. 5. (color online). Rational function fits of pseudo-data tables generated with nine models.

D. Fits with Continued Fractions

Using Continued Fraction, CF, expansions to fit G_E vs. Q^2 data was proposed and applied to the world data by Sick in 2003 [43]. This work also included tests and discussions regarding fitting pseudo and real data with CF expansions.

Fig. 6 summarizes results using the CF fit at order 1, 2, 3 and 4, with the same nine generating models. In these tests (using PRad binning), the second order CF is robust: $|\delta R| < \sigma$, regardless of the parameterizations in the generator, and the fitting uncertainties are small. Higher-order CF fitters, while robust ($|\delta R| < \sigma$ for all input G_E models), have significantly larger fitting uncertainties.

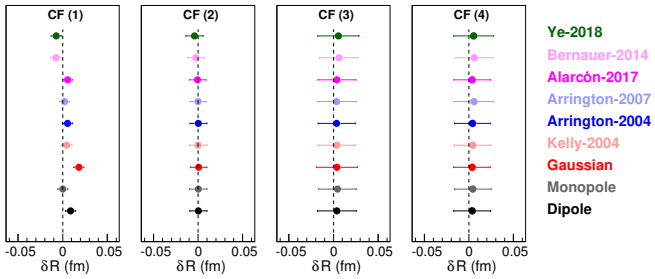

FIG. 6. (color online). CF fits of pseudo-data tables generated with nine G_E models.

E. Fits with polynomial expansions of z

Using polynomial expansion of z instead of Q^2 is another option to extract R. Here Eq. (19) is used to transform Q^2 to z.

Fig. 7 summarizes the fitting results using polynomial expansions of z with $N = 1$, 2, 3 and 4, using the nine generator functions. When $N = 1$, R(mean) is systematically and significantly larger than R(input) for all the generators used in the tests, opposite to the systematically smaller R(mean) for the polynomial (1) fits in Q^2. Again, as higher-order terms are included in the polynomial expansion of z, the bias is reduced though sigma increases. The polynomial expansion of z with $N = 2$ is clearly the best as it is robust and has a small fitting uncertainty.

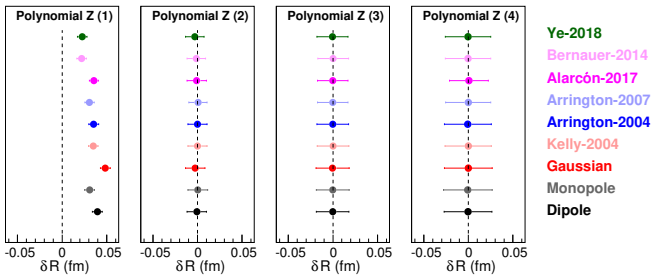

FIG. 7. (color online). Polynomial-expansions-of-z fits of pseudo-data tables generated with nine models.

IV. TESTS OVER LOW Q^2 SUBSETS OF THE PRAD KINEMATICS

In this section, we consider extracting R using only low Q^2 subsets of the PRad kinematics. As the amount of data in the extremely low Q^2 ranges are quite limited, it is easy to overfit the data and cause huge variances, so only the fit functions that give reasonable results are shown.

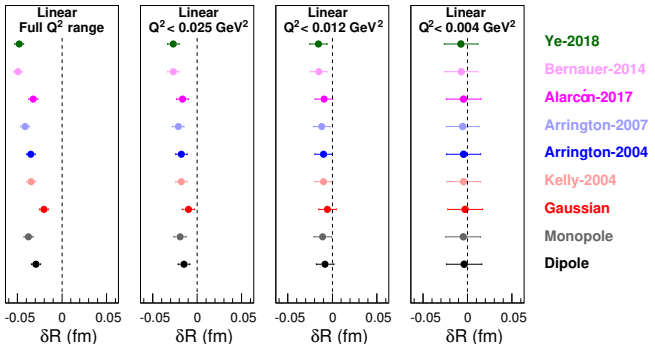

FIG. 8. (color online). The figure shows that while low Q^2 linear fits have a large bias when used full range; as the range in Q^2 is decrease, the bias decreases while the sigma increases.

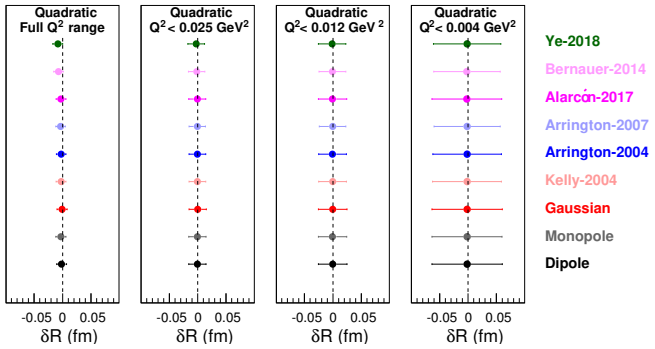

FIG. 9. (color online). A series of quadratic fits over low Q^2 ranges showing that for the smallest ranges the variance gets huge and the function overfits the data.

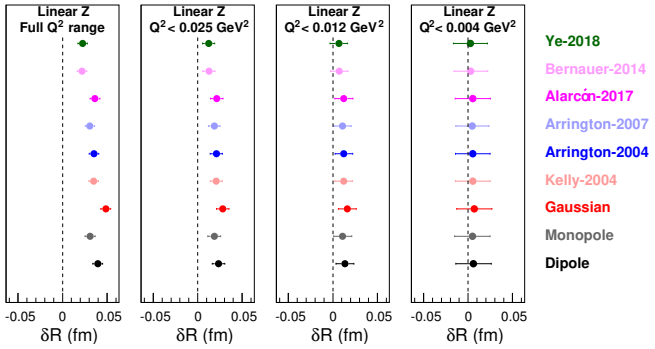

FIG. 10. (color online). Shown is a series of linear fits in z; again showing a trade-off between bias and variance as the upper limit in Q^2 is decreased.

Fig. 8, we show linear fits, first order polynomial, for various range of Q^2. For the full Q^2 range, the linear fit produces a large bias and has a poor residual, while as the range of the data is reduced, the linear fit becomes robust. In Fig. 9, we show that though the quadratic fits works reasonably well over the full range of the expect data, as the range is restricted the quadratic function quickly starts to overfit the data and has a much larger variance than the linear fits.

Repeating the linear fits in z instead of Q^2, again has the interesting effect that the bias has the opposite sign. Nevertheless, as the Q^2 range is decreased, the bias is reduced and the linear fits in both G_E vs. Q^2 and G_E vs. z agree. This emphasizes that merely transforming to z does not eliminate the problem of selecting the appropriate functional form to fit the data. Though the results do show that for very low Q^2, linear fits in z and Q^2 should agree.

V. DISCUSSION

Choosing the appropriate fit function to extract R for a given set of data depends on both the Q^2 ranges and bin-by-bin uncertainties, thus, the the choice of appropriate fitting function(s) needs to be determined on a case-by-case basis. In fact, Figs. 8 and 9 show that it is possible that simpler fitters are robust and have smaller σ then more complex functions when focusing low-Q^2 subsets of data. It is therefore imperative to define the criteria for selecting functions for extracting R.

A standard way of quantifying goodness of fit for this type of study where the true values are known is to consider both the bias and variance [48] using Root Mean Square Error, RMSE, where

$$\mathrm{RMSE} = \sqrt{\mathrm{bias}^2 + \sigma^2}. \tag{21}$$

In this study, δR is the bias and σ is represented by the RMS value of the fitting results.

Fig. 11 summarizes the bias, σ and RMSE values for the three good fitting functions, one of the large-bias fitters (dipole) and one of the large-variance fitters [polynomial expansion of z $(N = 4)$] for the full range of the expected PRad data. The RMSE values of the three good fitters are similar for all generating functions. The RMSE values of the large-bias fitter, though smaller than those of the three good fitters on average, have large variations when different generators are used, which indicates that the fitter is not robust. The RMSE values of the large-variance fitter are significantly larger than those of the good fitters, which indicates that too many parameters were used.

The G_E values in real data inevitably have some fluctuations around the true central value due to statistical and systematic uncertainties. To test if these fluctuations have been correctly accounted for in the tests herein, we check the distribution of our results against an ideal probability density function. The left panel of Fig. 12 shows the correlation between the χ^2 per degree of freedom (DOF) and $[R(\mathrm{fit}) - R(\mathrm{input})]$, where $\mathrm{DOF} = N(\mathrm{data}) - 2$, and $N(\mathrm{data})$ is the number of data points in the G_E vs. Q^2 table. The black curve in the right panel of Fig. 12 is the ideal probability density function of χ^2/DOF distribution, and the red curve is from the numerical tests. The good agreement between these two curves indicates that the tests work as expected [49, 50]. In this figure, both the generator and the fitter use the dipole functional form, though similar results were achieved for all functional forms.

The value of R extracted from a known generator can vary due to fluctuations even if the χ^2/DOF is reasonable. Additionally, a good χ^2 value is not sufficient to determine if the corresponding fit can extrapolate the radius properly. From a purely mathematical point of view, this can be understood as the difference between a good interpolating function, valid over the range of the data, and a functional form that can be used to extrapolate beyond the range of the data.

For, with real data, with one only a single data set and an unknown functional form, it is not possible to know exactly how much the fluctuations affect the R extraction unless R is already known precisely. On the other

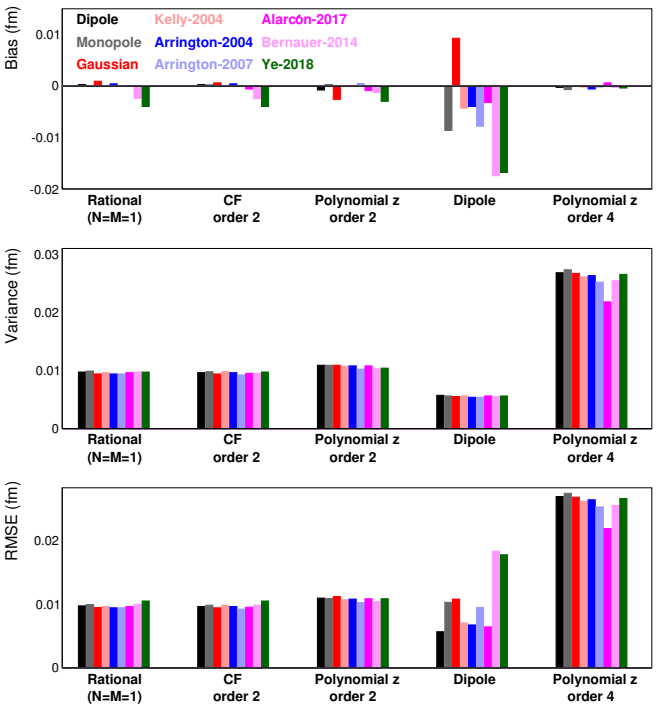

FIG. 11. (color online). Bias (δR), variance (σ) and RMSE of the rational ($N = 1, M = 1$), CF (second order), polynomial expansion of z ($N = 2$), dipole and polynomial expansion of z ($N = 4$) fitters. The last two fitters represent typical cases of under-fit (large bias and small variance) and over-fit (small bias and large variance), respectively. The bias, σ and RMSE values of nine G_E generators with the fitters presented by the nine colored columns in the corresponding to dipole, monopole, Gaussian, Kelly-2004, Arrington-2004, Arrington-2007, Alarcón-2017, Bernauer-2014 and Ye-2018 respectively.

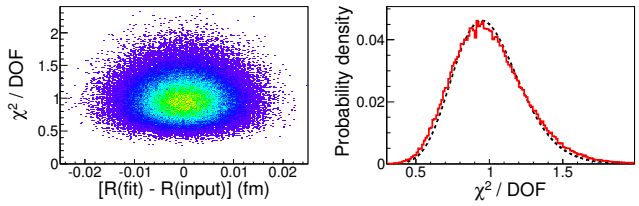

FIG. 12. (color online). The left panel presents the correlation between χ^2/DOF and $[R(\text{fit}) - R(\text{input})]$, when both the generator and the fitter use the dipole functional form. The black dashed curve in the right panel presents the ideal probability density function of χ^2/DOF distribution, and the red curve is from the numerical tests.

hand, one can make use of the statistical bootstrap which uses sampling with replacement to produce multiple data tables from a single set of data [51, 52]. While the bootstrap won't affect the mean, it allows determination of the uncertainty distribution from the data itself.

Theoretical models, such as Alarcón-2017, can also be used to help with fitting experimental data and extracting R. For example, one can use theory to constrain high order moments and achieve a smaller fit uncertainties [17], though these approaches inevitably introduce theory dependence to the R extraction. Theory dependence has been avoided in this study and we have demonstrated that the robust fitting functions are able to extract R by using relatively simple functions and treating the higher order moments as nuisance parameters. Of course, a pure mathematical extraction, such as demonstrated in this paper, and a valid nuclear theory extraction should give the same radius within errors.

VI. SUMMARY

We have created an expandable framework to search for functional forms that can reliably extract the proton radius using pseudo-data generated from a wide variety of G_E models. As a pertinent example, we have applied this framework to the expected range and uncertainty of the upcoming PRad data.

We find that for the full range of the data, the $(N = M) = (1, 1)$ rational function, the two parameter continued fraction, and the second order polynomial expansion in z can all robustly extract the correct radius with small σ regardless of the input pseudo-data generating function. By restricting data to the lowest Q^2 ranges, it is also possible to extract the radius using a linear function though this yields a larger uncertainty than when using the full range. We also note that functions with a good χ^2 do not necessarily extrapolate well beyond data; thus χ^2 alone cannot be used to determine which functions can robustly extract the proton radius.

ACKNOWLEDGMENTS

This work is supported by the U.S. Department of Energy, Office of Science, Office of Nuclear Physics under contract DE-AC05-060R23177 and supported in part by the U.S. Department of Energy under Contract No. DE-FG02-03ER41231, Thomas Jefferson National Accelerator Facility and Duke University. We acknowledge the helpful discussions with Jose Alarcón, John Arrington, Carl Carlson, Keith Griffioen, Ingo Sick, Simon Širca, Christian Weiss and Zhihong Ye. We also acknowledge the support and encouragement from Robert D. McKeown.

[1] R. Pohl *et al.*, Nature **466**, 213 (2010).

[2] A. Antognini *et al.*, Science **339**, 417 (2013).

[3] P. J. Mohr, D. B. Newell, and B. N. Taylor, Rev. Mod. Phys. **88**, 035009 (2016), arXiv:1507.07956 [physics.atom-ph].

[4] R. Pohl, R. Gilman, G. A. Miller, and K. Pachucki, Ann. Rev. Nucl. Part. Sci. **63**, 175 (2013), arXiv:1301.0905 [physics.atom-ph].

[5] C. E. Carlson, Prog. Part. Nucl. Phys. **82**, 59 (2015), arXiv:1502.05314 [hep-ph].

[6] R. J. Hill, *Proceedings, 12th Conference on Quark Confinement and the Hadron Spectrum (Confinement XII): Thessaloniki, Greece*, EPJ Web Conf. **137**, 01023 (2017), arXiv:1702.01189 [hep-ph].

[7] M. Mihovilovic *et al.*, Phys. Lett. **B771**, 194 (2017), arXiv:1612.06707 [nucl-ex].

[8] A. Beyer, L. Maisenbacher, A. Matveev, R. Pohl, K. Khabarova, A. Grinin, T. Lamour, D. C. Yost, T. W. Hänsch, N. Kolachevsky, and T. Udem, Science **358**, 79 (2017).

[9] H. Fleurbaey, S. Galtier, S. Thomas, M. Bonnaud, L. Julien, F. m. c. Biraben, F. m. c. Nez, M. Abgrall, and J. Guéna, Phys. Rev. Lett. **120**, 183001 (2018), 1801.08816 [physics.atom-ph].

[10] M. A. Belushkin, H. W. Hammer, and U. G. Meissner, Phys. Rev. **C75**, 035202 (2007), arXiv:hep-ph/0608337 [hep-ph].

[11] I. T. Lorenz, H. W. Hammer, and U.-G. Meissner, Eur. Phys. J. **A48**, 151 (2012), arXiv:1205.6628 [hep-ph].

[12] I. T. Lorenz and U.-G. Meiner, Phys. Lett. **B737**, 57 (2014), arXiv:1406.2962 [hep-ph].

[13] I. T. Lorenz, U.-G. Meiner, H. W. Hammer, and Y. B. Dong, Phys. Rev. **D91**, 014023 (2015), arXiv:1411.1704 [hep-ph].

[14] K. Griffioen, C. Carlson, and S. Maddox, Phys. Rev. **C93**, 065207 (2016), arXiv:1509.06676 [nucl-ex].

[15] D. W. Higinbotham, A. A. Kabir, V. Lin, D. Meekins, B. Norum, and B. Sawatzky, Phys. Rev. **C93**, 055207 (2016), arXiv:1510.01293 [nucl-ex].

[16] M. Horbatsch and E. A. Hessels, Phys. Rev. **C93**, 015204 (2016), arXiv:1509.05644 [nucl-ex].

[17] M. Horbatsch, E. A. Hessels, and A. Pineda, Phys. Rev. **C95**, 035203 (2017), arXiv:1610.09760 [nucl-th].

[18] J. Arrington and I. Sick, J. Phys. Chem. Ref. Data **44**, 031204 (2015), arXiv:1505.02680 [nucl-ex].

[19] G. Lee, J. R. Arrington, and R. J. Hill, Phys. Rev. **D92**, 013013 (2015), arXiv:1505.01489 [hep-ph].

[20] D. Borisyuk, Nucl. Phys. **A843**, 59 (2010), arXiv:0911.4091 [hep-ph].

[21] K. M. Graczyk and C. Juszczak, Phys. Rev. **C90**, 054334 (2014), arXiv:1408.0150 [hep-ph].

[22] J. C. Bernauer *et al.* (A1), Phys. Rev. Lett. **105**, 242001 (2010), arXiv:1007.5076 [nucl-ex].

[23] J. C. Bernauer *et al.* (A1), Phys. Rev. **C90**, 015206 (2014), arXiv:1307.6227 [nucl-ex].

[24] I. Sick and D. Trautmann, Phys. Rev. **C95**, 012501 (2017), arXiv:1701.01809 [nucl-ex].

[25] I. Sick, Atoms **6**, 2 (2018), arXiv:1801.01746 [nucl-ex].

[26] J. M. Alarcón and C. Weiss, Phys. Rev. **C97**, 055203 (2018), arXiv:1710.06430 [hep-ph].

[27] E. Kraus, K. E. Mesick, A. White, R. Gilman, and S. Strauch, Phys. Rev. **C90**, 045206 (2014), arXiv:1405.4735 [nucl-ex].

[28] A. Gasparian (PRad at JLab), *Proceedings, 13th International Conference on Meson-Nucleon Physics and the Structure of the Nucleon (MENU 2013): Rome, Italy, September 30-October 4, 2013*, EPJ Web Conf. **73**, 07006 (2014).

[29] C. Peng and H. Gao, *Proceedings, 21st International Conference on Few-Body Problems in Physics (FB21): Chicago, IL, USA, May 18-22, 2015*, EPJ Web Conf. **113**, 03007 (2016).

[30] G. Shmueli, Statist. Sci. **25**, 289 (2010).

[31] *Proton radius fitting library*, url: `https://github.com/saberbud/Proton_radius_fit_class`.

[32] R. Brun and F. Rademakers, Nucl. Instrum. Meth. **A389**, 81 (1997).

[33] F. James and M. Roos, Comput. Phys. Commun. **10**, 343 (1975).

[34] F. Borkowski, G. G. Simon, V. H. Walther, and R. D. Wendling, Zeitschrift für Physik A Atoms and Nuclei **275**, 29 (1975).

[35] J. J. Kelly, Phys. Rev. **C70**, 068202 (2004).

[36] J. Arrington, Phys. Rev. **C69**, 022201 (2004), arXiv:nucl-ex/0309011 [nucl-ex].

[37] J. Arrington and I. Sick, Phys. Rev. **C76**, 035201 (2007), arXiv:nucl-th/0612079 [nucl-th].

[38] S. Venkat, J. Arrington, G. A. Miller, and X. Zhan, Phys. Rev. **C83**, 015203 (2011), arXiv:1010.3629 [nucl-th].

[39] J. C. Bernauer, Ph.D. thesis, Johannes Gutenberg-Universitat Mainz (2010).

[40] J. M. Alarcón and C. Weiss, Phys. Rev. **C96**, 055206 (2017), arXiv:1707.07682 [hep-ph].

[41] J. M. Alarcón and C. Weiss, (2018), arXiv:1803.09748 [hep-ph].

[42] Z. Ye, J. Arrington, R. J. Hill, and G. Lee, Phys. Lett. **B777**, 8 (2018), arXiv:1707.09063 [nucl-ex].

[43] I. Sick, Phys. Lett. **B576**, 62 (2003), arXiv:nucl-ex/0310008 [nucl-ex].

[44] *PRad bin-set files*, url: `https://github.com/saberbud/Proton_radius_fit_class/tree/master/Bin_sets`.

[45] T. Hastie, R. Tibshirani, and J. Friedman, *The elements of statistical learning: data mining, inference and prediction*, 2nd ed. (Springer, 2009).

[46] T. B. Hayward and K. A. Griffioen, (2018), arXiv:1804.09150 [nucl-ex].

[47] A. J. R. Puckett *et al.*, Phys. Rev. **C96**, 055203 (2017), arXiv:1707.08587 [nucl-ex].

[48] T. Hastie, R. Tibshirani, and J. Friedman, *The elements of statistical learning: data mining, inference and prediction*, 2nd ed. (Springer, 2009).

[49] S. Sirca and M. Horvat, *Computational Methods for Physicists: Compendium for Students*, Graduate Texts in Physics (Springer Berlin Heidelberg, 2012).

[50] S. Širca, *Probability for Physicists*, Graduate Texts in Physics (Springer International Publishing, 2016).

[51] B. Efron, Ann. Stat. **7**, 1 (1979).

[52] B. Efron, J. Am. Stat. Assoc. **82**, 171 (1987).